

# Real-Time Transient Simulation Based on a Robust Two-Layer Network Equivalent

Xin Nie, *Student Member, IEEE*, Yuan Chen, *Student Member, IEEE*, and Venkata Dinavahi, *Member, IEEE*

**Abstract**—Real-time digital simulation of large power systems requires not only significant computational power but also simpler and accurate models. This paper proposes a new approach for transient simulation of power systems using a robust two-layer network equivalent model and an advanced PC-Cluster based parallel real-time simulator. Using a combination of well established fitting and optimization methods, the generated low-order model is of high accuracy compared to its full model over a wide frequency bandwidth. The merits of this method are its robustness in terms of stability and positive-realness, its accuracy at not only transient frequencies but also at dc and power frequency, and its optimal order determination feature. To validate the new method, a realistic large-scale power system—the Alberta Interconnected Electric System—is simulated in real-time. The real-time electromagnetic transient program is implemented in C++ language using object-oriented programming techniques on the PC-Cluster. A time-step of 20  $\mu$ s has been used for the real-time simulation. The captured oscilloscope results demonstrate excellent accuracy and efficiency of the proposed model in comparison to a full-scale off-line simulation of the original system in the ATP version of EMTF.

**Index Terms**—Electromagnetic analysis, frequency domain analysis, object oriented programming, power system transients, real-time systems, transmission lines.

## I. INTRODUCTION

REAL-TIME simulation plays an important role in the design and development of power systems for the closed-loop testing of protective relays and digital controllers. Although it is desirable to represent the whole power system in great detail, it is not always practical to do so due to excessive computational burden. In electromagnetic transient studies [1], due to system complexities, it is a common practice to divide the system into a *Study Zone*, a restricted part of the system where the transient phenomena occur and whose components must be fully characterized including any nonlinear and time-variant elements, and an *External System* which encompasses the rest of the system (Fig. 1). Since high frequency electromagnetic waves propagate short electrical distances because of high attenuation, therefore, the external system is represented by a

Manuscript received October 9, 2006; revised August 8, 2007. This work was supported by the Natural Science and Engineering Research Council of Canada (NSERC). Paper no. TPWRS-00681-2006.

X. Nie is with the SNC-Lavalin T & D, Calgary, AB T2G 4Y5, Canada (e-mail: xn timer@ece.ualberta.ca).

Y. Chen and V. Dinavahi are with the Department of Electrical and Computer Engineering, University of Alberta, Edmonton, AB T6G 2V4, Canada (e-mail: yuanchen@ece.ualberta.ca; dinavahi@ece.ualberta.ca).

Color versions of one or more of the figures in this paper are available online at <http://ieeexplore.ieee.org>.

Digital Object Identifier 10.1109/TPWRS.2007.907963

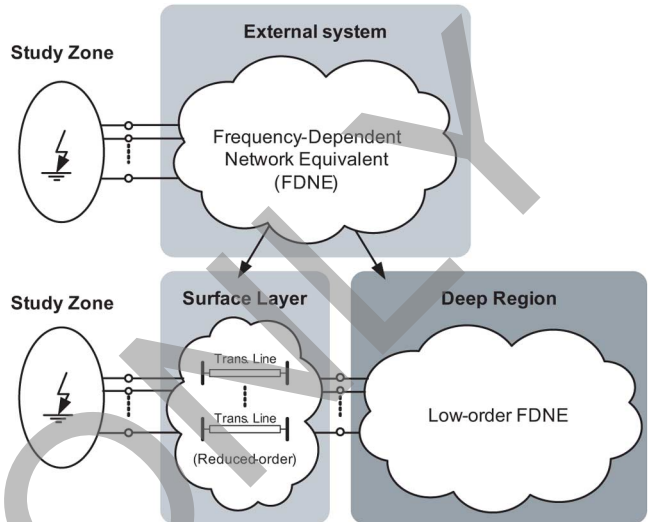


Fig. 1. Two-Layer Network Equivalent for the external system.

linear equivalent network, i.e., a Frequency-Dependent Network Equivalent (FDNE) [2], [3]. The latest development in constructing FDNE is the vector fitting technique [4], [5].

For real-time transient simulation of large power systems, however, the computational bottleneck still remains due to the efficiency concern in convolutions and the high order of the fitted FDNE model of external systems. The Two-Layer Network Equivalent (TLNE) (Fig. 1), first proposed in [6], is another development in overcoming this obstacle for real-time digital simulation. In the TLNE, the external system is further partitioned into a *Surface Layer* represented by reduced-order frequency-dependent transmission line models and a *Deep Region* represented as a low-order FDNE. The impact of Surface Layer and Deep Region on the external system input admittance varies with frequency. At low frequencies, both the Surface Layer and Deep Region contribute to the input admittance. When the frequency increases, however, the contribution of the Deep Region diminishes drastically due to high attenuation. Therefore, the FDNE model for the Deep Region is able to be obtained in low order.

Existing methods in [6] for obtaining TLNE rely on low-order vector fitting for both Surface Layer and Deep Region parameters, and Sequential Quadratic Programming (SQP) to ensure passivity of the model. Nonetheless, the following concerns were revealed in our experience [7], [8] with this method:

- 1) With low-order vector fitting in obtaining the Deep Region, it is difficult to control deviations with respect to the original Deep Region, which SQP may not be able to compensate.

- 2) Frequency response at dc is not specifically accentuated although it affects the dc offset in the transient. Optimization of the Surface Layer can help in increasing accuracy of response in the low frequency range with little cost of computational time.
- 3) SQP is prone to divergence. If better first approximations of external system input admittance, which are both stable and passive, can be found, then SQP can be replaced by constrained nonlinear least-square optimization, which gives improved convergence.
- 4) In multi-port external systems with complex frequency response, the passivity constraint is very strong, so the freedom for changing the parameters is small. Therefore, the first approximation in a multi-port case, is required to be closer to the original than that for the single-port case. Thus, transmission line parameters in the Surface Layer require higher accuracy but low-order realization.

In this paper, we propose real-time simulation of power systems based on a Robust Two-Layer Network Equivalent. Its features include low-order Marti's frequency-dependent line model in Surface Layer, global searching of low-order Deep Region networks by genetic algorithms, and constrained nonlinear least-square optimization with improved convergence, as well as the stability and passivity of the obtained model. The Robust TLNE is introduced in Section II. Section III presents a detailed case study of a realistic, large power system- the Alberta Interconnected Electric System- as well as off-line time-domain results from ATP to show the effectiveness of the proposed approach. A close agreement of the full model and the Robust TLNE model of the system has been obtained. A real-time EMTP has been implemented on a PC-Cluster [9] using C++ language and object-oriented programming techniques. Section IV describes this implementation and also shows the real-time transient simulation results. Conclusions are given in Section V.

## II. ROBUST TWO-LAYER NETWORK EQUIVALENT

### A. Background

The robustness of a network is determined not only by its stability, i.e., transfer function of admittance matrix with stable poles, but also by its passivity, or positive-realness [5]. A passive network must absorb active power at any frequency when any set of voltages are applied. The passivity criterion is of equal importance to stability due to its strong effect on the stableness of time-domain simulations; the electric network with passivity violations will most likely result in unstable and erroneous simulations. For a network represented by the nodal equation

$$\mathbf{YV} = \mathbf{I} \quad (1)$$

the passivity criterion requires that the real part of the input admittance  $\mathbf{Y}$  be positive at all frequencies for a single-port network, or all eigenvalues of the real part of the input admittance matrix  $\mathbf{Y}$  be positive in the entire frequency range for a multi-port network.

In the existing TLNE method, both the approximation of Surface Layer admittance  $\mathbf{Y}_{\text{surface}}(\omega)$  and Deep Region admittance

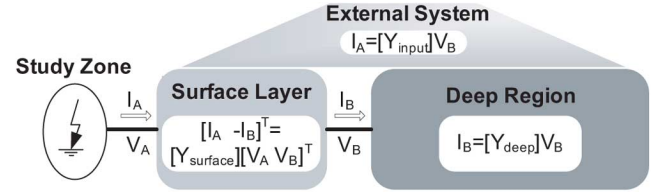


Fig. 2. Admittance matrix for the TLNE external system.

$\mathbf{Y}_{\text{deep}}(\omega)$  are obtained from low-order vector fitting. Then the input admittance  $\mathbf{Y}_{\text{input}}(\omega)$  of external system is obtained by combining  $\mathbf{Y}_{\text{surface}}(\omega)$  and  $\mathbf{Y}_{\text{deep}}(\omega)$  as shown in Fig. 2. However, using vector fitting alone can not always ensure a relatively good approximation especially for an external system with complicated frequency response over a wide frequency bandwidth. It is necessary to find out alternate methods that are able to generate better approximations for the TLNE. In the Robust TLNE, genetic algorithms are used to find out the best low-order Deep Region  $\mathbf{Y}_{\text{deep}}(\omega)$  approximation which can minimize the deviation of external system input admittance  $\mathbf{Y}_{\text{input}}(\omega)$  approximation. Further improvement is achieved by constrained nonlinear least-square optimization with the inclusion of frequency response at dc and the optimal Deep Region order determination feature.

In this paper, application of the Robust TLNE model is limited only to a balanced external system, i.e., one that includes fully transposed transmission line models in the Surface Layer and a balanced FDNE model in the Deep Region. With Clarke's modal transformation [10], the external system can then be decoupled into two aerial modes ( $\alpha, \beta$ ) of identical passive parts and one ground mode (0). The Robust TLNE procedure is applied only to the aerial modes, since the FDNE model is sufficient for fitting the ground mode frequency response due to its relative smoothness.

### B. Surface Layer

The Surface Layer consists of reduced-order frequency-dependent transmission line models. In the Robust TLNE model, Marti's frequency-dependent line model [12] is employed since it is widely used and its low-order realization [13], [14] has been shown to be suitable for real-time implementation [15], [16]. It is based on the well-known line model equations in frequency-domain

$$V_k(\omega) = \cosh[\gamma(\omega)\ell]V_m(\omega) - Z_c(\omega)\sinh[\gamma(\omega)\ell]I_m(\omega) \quad (2a)$$

$$I_k(\omega) = \frac{1}{Z_c(\omega)}\sinh[\gamma(\omega)\ell]V_m(\omega) - \cosh[\gamma(\omega)\ell]I_m(\omega) \quad (2b)$$

where  $V_k(\omega)$ ,  $V_m(\omega)$ ,  $I_k(\omega)$ , and  $I_m(\omega)$  are the voltages and currents corresponding to the sending-end ( $k$ ) and receiving-end ( $m$ ), respectively;  $\ell$  is the line length;  $Z_c(\omega)$  and  $\gamma(\omega)$  are the frequency-dependent characteristic impedance and propagation function, respectively, defined as

$$Z_c(\omega) = \sqrt{\frac{R(\omega) + j\omega L(\omega)}{G + j\omega C}} \quad (3a)$$

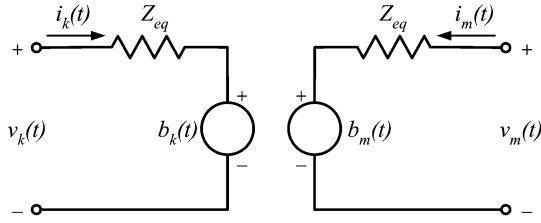


Fig. 3. Marti's frequency-dependent line model [12].

$$\gamma(\omega) = \sqrt{(R(\omega) + j\omega L(\omega))(G + j\omega C)} \quad (3b)$$

where  $R(\omega)$ ,  $L(\omega)$ ,  $G$ ,  $C$  are series resistance, series inductance, shunt conductance, and shunt capacitance, respectively.

By introducing forward traveling functions  $F_k(\omega)$  and  $F_m(\omega)$ , backward traveling functions  $B_k(\omega)$  and  $B_m(\omega)$ , and weighting function  $A_1(\omega)$ , (2a) and (2b) give the Thevenin equivalent network as shown in Fig. 3. where the  $Z_{eq}$  is the impedance of equivalent network approximating  $Z_c(\omega)$ ; the voltage sources  $b_k(t)$  and  $b_m(t)$  are the time-domain forms of  $B_k(\omega)$  and  $B_m(\omega)$ .

The accuracy of Marti's line model greatly depends on the fitting of impedance function  $Z_c(\omega)$  and weighting function  $A_1(\omega)$ . The appropriate techniques used in this paper are Bode's asymptotic fitting technique [12] and nonlinear Levenberg-Marquardt (LM) fitting method [14]. We preferred the non-linear LM fitting method due to its improved accuracy and speed.

From individual lines which have the nodal (2a) and (2b), the admittance matrix of the reduced-order Surface Layer network can be constructed as follows:

$$\tilde{\mathbf{Y}}_{\text{surface}}(\omega) = \begin{bmatrix} \tilde{\mathbf{Y}}_{AA}(\omega) & \tilde{\mathbf{Y}}_{AB}(\omega) \\ \tilde{\mathbf{Y}}_{BA}(\omega) & \tilde{\mathbf{Y}}_{BB}(\omega) \end{bmatrix} \quad (4)$$

where subscript  $A$  stands for the ports connected to the Study Zone, subscript  $B$  stands for the ports connected to the Deep Region (Fig. 2), and  $\tilde{\phantom{x}}$  designates simplification or approximation.

### C. Deep Region

The fitting of external system by vector fitting is stressed on relatively lower frequency range since high frequency transients do not travel very far in the external system. In the TLNE, the Deep Region is further "insulated" from the Study Zone by the Surface Layer. Thus, the order of Deep Region can be significantly reduced.

The first approximation of external system input admittance  $\tilde{\mathbf{Y}}_{\text{input}}^0(\omega)$  is the initial mathematical combination of admittance matrix  $\tilde{\mathbf{Y}}_{\text{surface}}(\omega)$  of the Surface Layer constituting reduced-order line models and  $\tilde{\mathbf{Y}}_{\text{deep}}(\omega)$  of the Deep Region comprising low-order FDNE

$$\tilde{\mathbf{Y}}_{\text{input}}^0(\omega) = \tilde{\mathbf{Y}}_{AA}^0(\omega) - \tilde{\mathbf{Y}}_{AB}^0(\omega) * \left[ \tilde{\mathbf{Y}}_{BB}^0(\omega) + \tilde{\mathbf{Y}}_{\text{deep}}^0(\omega) \right]^{-1} \tilde{\mathbf{Y}}_{BA}^0(\omega) \quad (5)$$

where the superscript  $^0$  denotes "first" since the subsequent optimizations are to be carried out;  $\tilde{\mathbf{Y}}_{AA}^0(\omega)$ ,  $\tilde{\mathbf{Y}}_{AB}^0(\omega)$ ,  $\tilde{\mathbf{Y}}_{BA}^0(\omega)$ ,

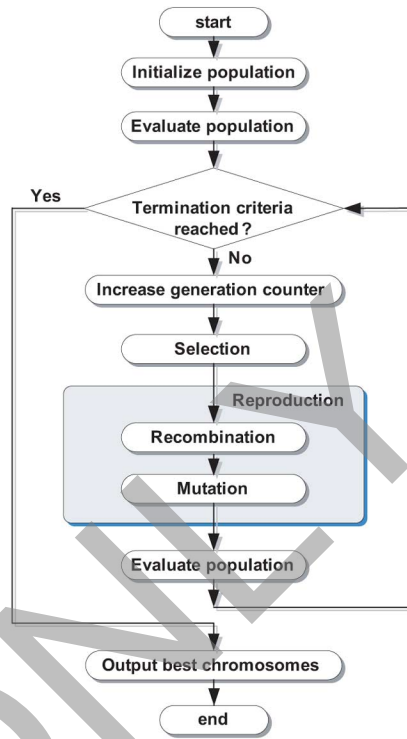


Fig. 4. Flowchart for genetic algorithms procedure.

and  $\tilde{\mathbf{Y}}_{BB}^0(\omega)$  corresponds to the blocks of the first approximation of Surface Layer admittance  $\tilde{\mathbf{Y}}_{\text{surface}}^0(\omega)$  in (4). The ultimate goal of building the Robust TLNE is to match  $\tilde{\mathbf{Y}}_{\text{input}}(\omega)$  with the original external system input admittance  $\mathbf{Y}_{\text{input}}(\omega)$  as close as possible while ensuring stability and passivity of the model, and accurate frequency response at dc and power frequency. The application of genetic algorithms plays a crucial role in constructing the Robust TLNE.

### D. Genetic Algorithms

The genetic algorithm is a probabilistic-rule based global search method mimicking natural biological evolution [11]. It is a generation-based algorithm which operates on a population of potential solutions or individuals. The flowchart in Fig. 4 illustrates the genetic algorithms procedure. The inputs of genetic algorithms are chromosomes, which are encoded decision variables (variables considered for optimization). Objective functions are used to assess the performance (fitness) of the individuals. Depending on the problem size and characteristics, a set of individuals or a population is first generated and evaluated by objective functions, and each individual is given a fitness value. At each generation, selection phase and reproduction phase are carried out. Reproduction phase commonly includes two steps: recombination and mutation. In the recombination step, operators are applied to exchange genetic information between pairs or groups of individuals. Mutation, which is used to converge genetic algorithms to global optimum, is applied to new chromosomes generated after recombination. It causes individual chromosomes to change according to probabilistic rules. Thus, in subsequent generations, genetic algorithms

produce better results by applying the principle of survival of the fittest.

The concept for finding reduced-order Deep Region is based on the fact that in frequency domain, each resonant peak of the original Deep Region admittance  $\mathbf{Y}_{\text{deep}}(\omega)$  is likely to produce a resonant peak in the input admittance of external system  $\mathbf{Y}_{\text{input}}(\omega)$ . However, due to the insulation of Surface Layer, some peaks in  $\mathbf{Y}_{\text{deep}}(\omega)$  are insensitive to  $\mathbf{Y}_{\text{input}}(\omega)$ . This gives the idea that removing some resonant peaks in Deep Region will have little effect on  $\mathbf{Y}_{\text{input}}(\omega)$ . Thus, a better first approximation can be found by globally selecting the resonant peaks of the original Deep Region that have more significant effect on  $\mathbf{Y}_{\text{input}}(\omega)$  in the designated low orders of the Deep Region FDNE model. This is a multi-variable multi-objective optimization problem with nonlinear passivity constraints, for which the genetic algorithms are well-suited. The partial fraction terms representing rational functions generated by full-order vector fitting are indexed and encoded as chromosomes, so that the genetic algorithms are able to find the best suitable partial fractions for the Deep Region. Further compensation is applied to eliminate deviation effects at lower frequencies in this procedure.

Since genetic algorithms try to find out the best low-order Deep Region  $\tilde{\mathbf{Y}}_{\text{deep}}^0(\omega)$  that minimizes the difference between  $\tilde{\mathbf{Y}}_{\text{input}}^0(\omega)$  and  $\mathbf{Y}_{\text{input}}(\omega)$  while ensuring  $\tilde{\mathbf{Y}}_{\text{deep}}^0(\omega)$  is positive-real, the objective function [11] for a  $m$ -port external system is defined as follows:

$$\begin{aligned} f_{obj} &= \left\| \mathbf{Y}_{\text{input}}(\omega) - \tilde{\mathbf{Y}}_{\text{input}}^0(\omega) \right\|_F^2 + \mu \\ &= \sum_{i,j=1}^m \left| \mathbf{Y}_{\text{input},ij}(\omega) - \tilde{\mathbf{Y}}_{\text{input},ij}^0(\omega) \right|^2 + \mu \end{aligned} \quad (6)$$

where  $\mathbf{Y}_{ij}(\omega)$  is the  $ij$ th element of the matrix  $\mathbf{Y}(\omega)$ ;  $\mu$  denotes a penalty term when the passivity criterion violation occurs in the Deep Region. If the criterion is violated,  $\mu$  will be a large positive number, or else  $\mu = 0$ . This ensures that the outputs from genetic algorithms are the best fitted Deep Regions, which are both stable and positive-real.

### E. Constrained Nonlinear Least-Square Optimization

Theoretically, the generated input admittance  $\tilde{\mathbf{Y}}_{\text{input}}^0(\omega)$  from genetic algorithms is very close to the original  $\mathbf{Y}_{\text{input}}(\omega)$ . Nonetheless, the reduced-order Surface Layer  $\tilde{\mathbf{Y}}_{\text{surface}}^0(\omega)$  and genetic algorithm generated Deep Region  $\tilde{\mathbf{Y}}_{\text{deep}}^0(\omega)$  are subject to further fine-tuning to minimize the deviations between  $\tilde{\mathbf{Y}}_{\text{input}}^0(\omega)$  and  $\mathbf{Y}_{\text{input}}(\omega)$ . In the Robust TLNE model, to ensure faster algorithm convergence and accuracy, the parameters considered for further optimization include the following.

- In the Surface Layer line models, constant terms, and all poles and residues of partial fraction form of the  $\tilde{Z}_c(s)$ , the transfer function approximating  $Z_c(\omega)$ . Weighting function  $A_1(s)$  parameters were not considered for optimization since they resulted in excessive convergence time.
- In the Deep Region FDNE models, all constant terms and residues of the first approximation of  $\tilde{\mathbf{Y}}_{\text{deep}}^0(s)$ .

In our experience [8], optimizing Surface Layer parameters particularly improves the frequency response at dc and power frequency with little cost of computational time. By building

the Jacobian matrix  $\mathbf{J}(\omega)$ , an iterative process is initiated by recursive evaluation of the following equation:

$$\mathbf{x} = \mathbf{x}_0 + \Delta \mathbf{x} \quad (7)$$

where  $\Delta \mathbf{x}$  is obtained by the overdetermined linear equation

$$\Delta \mathbf{Y}_{\text{input}}(\omega) = \mathbf{J}(\omega) \Delta \mathbf{x} \quad (8)$$

$\mathbf{x}$  is the model parameter column vector considered for optimization, and  $\Delta \mathbf{x}$  is the model parameter change column vector. Since the process only accepts real quantities, real and imaginary parts in  $\Delta \mathbf{Y}_{\text{input}}(\omega)$  are separated in (8). Therefore, (8) is replaced as

$$\begin{bmatrix} \text{Re}(\Delta \mathbf{Y}_{\text{input}}(\omega)) \\ \text{Im}(\Delta \mathbf{Y}_{\text{input}}(\omega)) \end{bmatrix} = \begin{bmatrix} \text{Re}(\mathbf{J}(\omega)) \\ \text{Im}(\mathbf{J}(\omega)) \end{bmatrix} \Delta \mathbf{x}. \quad (9)$$

Appendix A explains how the Jacobian matrix  $\mathbf{J}(\omega)$  is obtained.

During the optimization, both the positive-real criterion and algorithm convergence must be guaranteed, which leads to the concept of constrained optimization. It has been discussed in [6] that SQP is required to accomplish this task after the unconstrained nonlinear least-square optimization. Consequently, (9) has to be converted to the more complex quadratic form. However, SQP method is prone to divergence and is computationally expensive. In the Robust TLNE, since genetic algorithms are able to obtain better first approximations that are both stable and passive, i.e., the first approximations are already in the feasible region in optimization sense and close to the original, only minor fine-tunings are required. Therefore, instead of SQP, constrained nonlinear least-square optimization is employed.

In each iteration of evaluating  $\Delta \mathbf{x}$ , both the stability and passivity conditions for the Surface Layer and Deep Region are verified after adding parameter changes. During the condition check, each transmission line in the Surface Layer and the whole Deep Region is treated as an individual entity. The entities with either condition violation lead to a positive number  $\delta$  ( $0 < \delta < 1$ ) being multiplied with their corresponding parameters change (a part of  $\Delta \mathbf{x}$ ), since they have changed too much. Another essential condition in the optimization is the decrease of RMS-error% in the model input admittance during subsequent iterations. If RMS-error% does not decrease compared to the last iteration, the whole parameter change vector  $\Delta \mathbf{x}$  is also multiplied by  $\delta$ . The optimal point or termination criterion is that for a consecutive number times the multiplication of  $\delta$  with  $\Delta \mathbf{x}$ , the RMS-error% of input admittance does not decrease. Therefore, (7) is re-written as shown in (10) at the bottom of the next page, where  $0 < q < N_{op}$ ,  $\Delta \mathbf{x}_1$  is parameter change of criterion violation, and  $\Delta \mathbf{x}_2$  is the parameter change not violating any criteria.

In order to obtain the best suitable order for Deep Region, a series of Deep Region orders are applied to the problem. Thus, a collection of discrete values representing the order of Deep Region versus RMS-error% is obtained. The optimal order is the one where for orders lower than it, the percentage RMS-error increases dramatically, whereas for orders higher than it, the percentage RMS-error does not decrease significantly. The case study in Section III illustrates this concept.



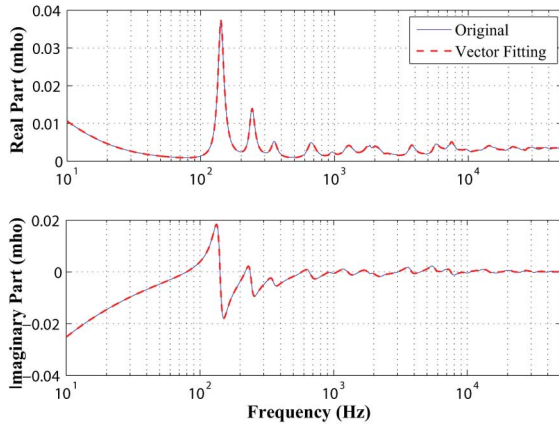


Fig. 7. AIES Area 50 ground mode input admittance  $Y_{\text{input},0}$ .

The transients to be analyzed are at Bus 524 (Genesee), which connects a number of generation stations together to the power grid of AIES. Since transients to be analyzed are at this bus, the generation stations are treated as the Study Zone and the rest of the network is considered as the external system. As shown in Fig. 6, after applying the Robust TLNE model to the external system, transmission lines 1202 L, 1203 L, 1209 L belong to the Surface Layer and the remainder forms the Deep Region.

Following the flowchart in Fig. 5, the frequency scan of passive Deep Region produces phase-domain admittance matrix, and short-circuit currents provide Norton equivalent current sources. The whole external system is considered balanced. Therefore, Clarke's modal transformation further decouples the phase-domain matrix into two aerial modes ( $\alpha, \beta$ ) of identical passive parts and one ground (0) mode. As shown in Fig. 7, due to ground return, the ground mode input admittance  $Y_{\text{input},0}(\omega)$  is relatively smooth. Full-order vector fitting generates a 36th order FDNE model with 1.28% RMS-error. Therefore, the Robust TLNE model is applied only to the aerial mode admittance since a very high-order rational function is required to achieve low RMS-error% in fitting input admittance  $Y_{\text{input},\alpha}$  by vector fitting, as shown in Fig. 8. For example, applying full-order vector fitting on original aerial mode Deep Region frequency response  $Y_{\text{deep},\alpha}$  generates a 240th order rational function matrix with 1.93% RMS-error. Thus, the external system model consists of

- Aerial mode of Robust TLNE model with one-port external system and two-port Deep Region;
- Ground mode of one-port FDNE model.

In fitting of Surface Layer transmission line parameters  $Z_c(\omega)$  and  $A_1(\omega)$ , non-linear Levenberg-Marquardt fitting technique [14] is used for the aerial mode. Combining the Surface Layer with the results computed by genetic algorithms, constrained nonlinear least-square optimization is applied to find the best suitable Deep Regions. Fig. 9 shows the element 11 frequency response of the Deep Region aerial mode matrix generated by genetic algorithms and the constrained nonlinear least-square optimization, respectively. Elements 12, 21, and 22 follow the same pattern. The RMS-error% of input admittance versus Deep Region order is shown in Fig. 10. The order of 25 is recognized as the optimal Deep Region order where with the

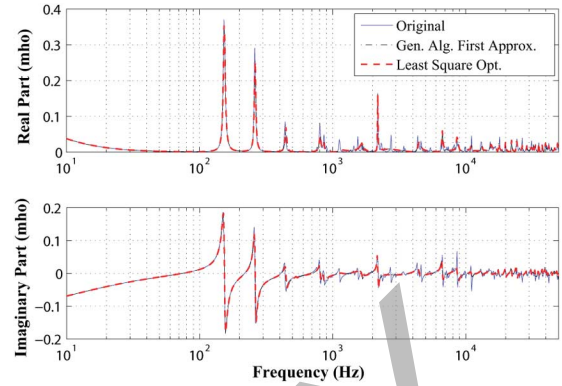


Fig. 8. AIES Area 50 aerial mode input admittance  $Y_{\text{input},\alpha}$ .

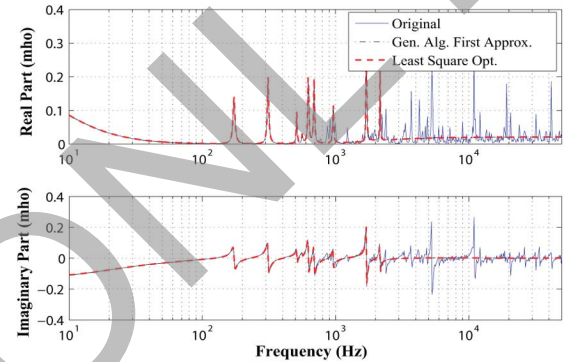


Fig. 9. AIES Area 50 aerial mode Deep Region admittance  $Y_{\text{deep},\alpha,11}$ .

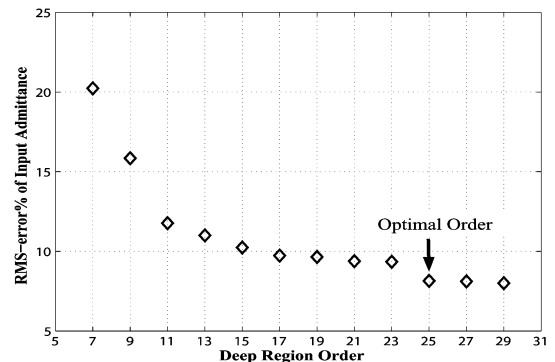


Fig. 10. AIES Area 50 aerial mode RMS-error% of input admittance versus Deep Region order.

higher orders of Deep Region, RMS-error% of input admittance does not decrease dramatically and is less than 10% (8.144%). It is shown that due to their relative insensitivity to the input admittance, a lot of pronounced resonant peaks in the deep region are eliminated by genetic algorithms, which demonstrates the salient feature of the new methodology in generating Robust TLNE. To achieve the same level of RMS-error% as that of the Robust TLNE, the FDNE model of the external system generated by vector fitting requires a 220th order rational function, which is much higher than the combined order of the Robust TLNE model. All the optimization codes were written using MATLAB script, which can make the generation of the Robust TLNE model time-consuming. However, since this process is done off-line, it is not a major concern. Significant computation

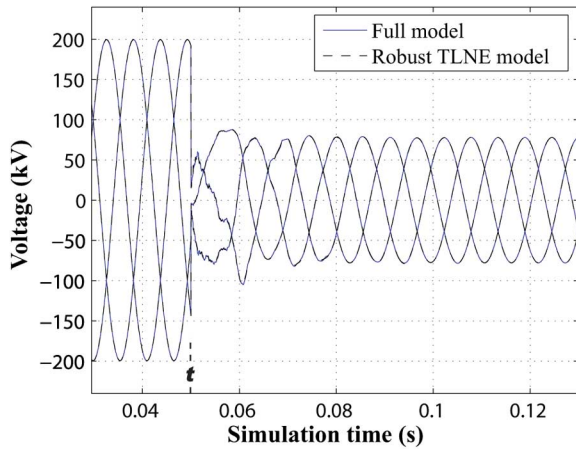


Fig. 11. Three-phase voltages at Bus 524 of the AIES Area 50 during a three-phase to ground fault transient at  $t = 0.05$  s.

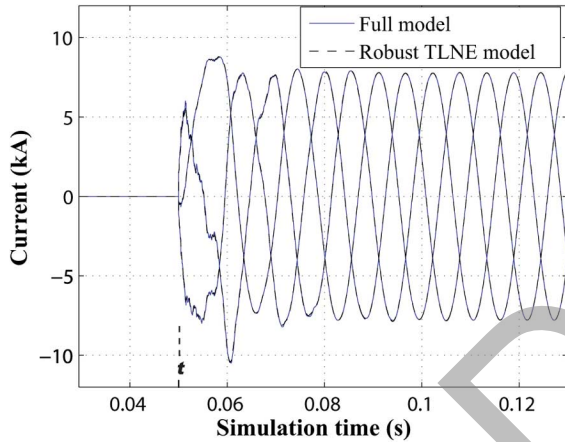


Fig. 12. Three-phase fault currents at Bus 524 of the AIES Area 50 during a three-phase to ground fault transient at  $t = 0.05$  s.

time saving can be expected by re-writing all optimization codes using compilable languages such as C or C++.

Figs. 11 and 12 show the three-phase voltage and current transients at Bus 524, respectively, when a balanced three-phase to ground fault with  $10 \Omega$  resistance occurs at  $t = 0.05$  s. The total simulation time is 0.15 s. All transients are verified using ATP with a time-step of  $20 \mu\text{s}$ . Detailed agreement between the full model of the system and the Robust TLNE model can be observed.

A harmonic current source  $i(t)$  given by (11) is injected at Bus 524 in the Study Zone during the times  $t_1 = 0.0331$  s to  $t_2 = 0.0664$  s. Fig. 13 shows the three-phase voltages at Bus 524 during this transient, while a detailed view of the high frequency components voltages from  $t_1 = 0.0331$  s to  $t = 0.0625$  s is shown in Fig. 14. Again, detailed agreement between the full system model and the Robust TLNE model can be seen in these figures.

$$i(t) = \left[ 0.5 \cos(2\pi(240)t) + 0.1 \cos(2\pi(3600)t) + 0.05 \cos(2\pi(18000)t) \right] \text{kA} \quad (11)$$

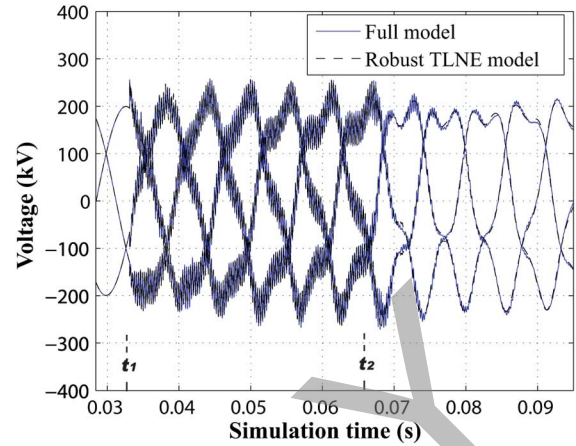


Fig. 13. Three-phase voltages at Bus 524 of the AIES Area 50 during a harmonic current injection transient between  $t_1 = 0.0331$  s and  $t_2 = 0.0664$  s.

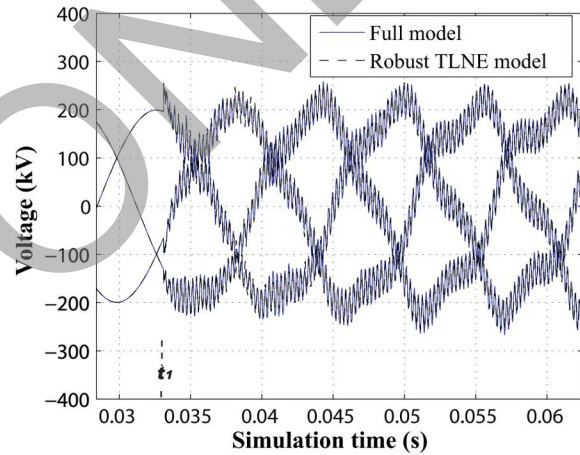


Fig. 14. Detailed view of transient in Fig. 13 from  $t_1 = 0.0331$  s to  $t = 0.0625$  s.

TABLE I  
OFF-LINE EXECUTION TIME COMPARISON WITH A SIMULATION TIME-STEP OF  $20 \mu\text{s}$

Total time	Full model	220th FDNE	Robust TLNE
0.15s	17.604s	0.352s	0.081s

Table I shows computational time comparison between the full model, the Robust TLNE model, and the FDNE model on the same Pentium IV 1.6 GHz computer. The 220th order FDNE model does demonstrate great saving in computational time. However, computational saving of the Robust TLNE model is much more substantial. As can be seen from Table I, the Robust TLNE model is about 50 times faster than the full model. In our experience [8], we found that the more complex the system, the larger the computational saving with the Robust TLNE model. It can also be seen that the simulation time of the Robust TLNE model is already well below 0.15 s. With the precalculation of the inverse of the system admittance matrix, more computational saving can be obtained for real-time implementation.

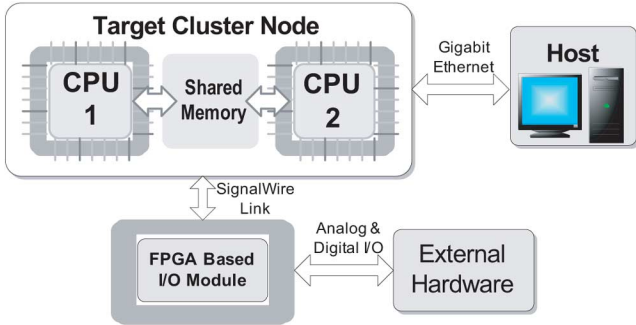


Fig. 15. Real-time simulator configuration.

#### IV. REAL-TIME SIMULATION

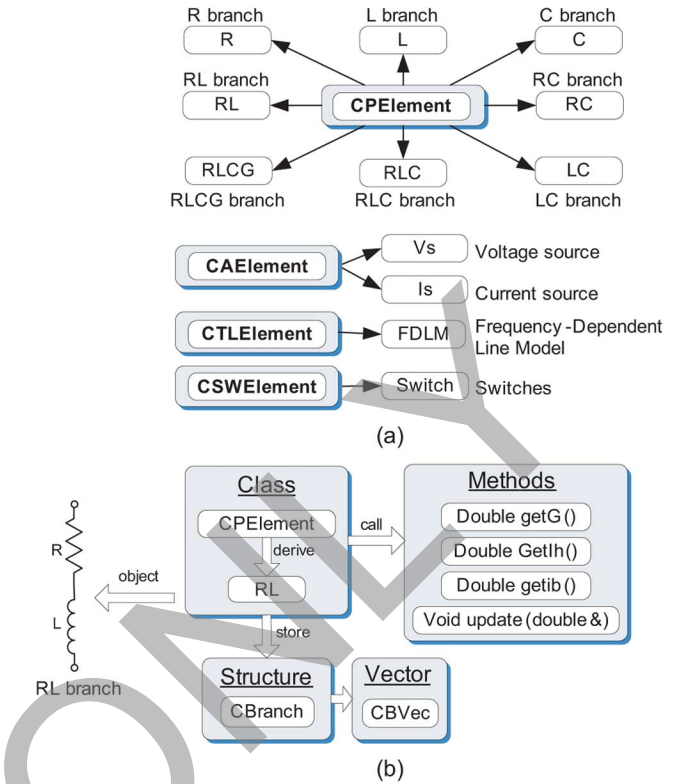
##### A. Simulator Configuration

The real-time simulator is based on an advanced PC-Cluster [9]. As shown in Fig. 15, the hardware mainly comprises of two groups of computers known as the *target*, and the *host* with a high-speed communication link between them. The external hardware is connected via FPGA-based analog/digital I/Os. The target is powered by dual 3.0 GHz Intel® Xeon™ processors that communicate with each other through shared memory. The target is also capable of extreme high performance mode execution, in which one CPU is dedicated entirely to computation while the other CPU runs the operating system. The target uses real-time Linux as the operating system to perform functions such as real-time execution of the model, data acquisition, and I/O communication. The host is a single-processor computer with a 3.0 GHz Intel® Pentium® IV CPU. It is installed with a real-time interfacing software called RT-LAB™ [17] to coordinate all hardware engaged in the simulation. The host is mainly used to create, edit and verify models in SIMULINK, compile SIMULINK blocks into C code, and to control and configure the real-time simulation in the target.

##### B. C++ Implementation of Real-Time EMTP

In MATLAB/SIMULINK, since Marti's frequency-dependent line model is not available, it is not straightforward to implement the Robust TLNE model using regular blocks from the SimPowerSystem Blockset in SIMULINK. Moreover, the models in MATLAB/SIMULINK are based on the state-space approach, whereas EMTP uses the nodal method [1]. Therefore, EMTP is implemented using a customized function block in SIMULINK. The SIMULINK S-function block, which can be implemented by C/C++ and Fortran programming languages in S-function code format [18] is well-suited for this scenario. For enhanced scalability and portability, the custom EMTP S-function is written in the C++ language using object-oriented programming techniques. The program mainly includes two parts: (1) reading the ATP data file with initializations, and (2) simulating the electrical network based on EMTP nodal solution.

In the C++ code, four base classes and their derivatives are defined for the real-time EMTP S-function as shown in Fig. 16(a): (1) CPElement for passive elements  $R$ ,  $L$ ,  $C$

Fig. 16. (a) C++ class hierarchy for EMTP (b) An example of  $RL$  branch in the C++ S-function.

and possible combinations such as  $RL$ ,  $RC$ ,  $LC$ ,  $RLC$ , and  $RLCG$ , (2) CAElement for active elements such as ideal voltage and current sources, (3) CTLElement for frequency-dependent transmission line model, and (4) CSWElement for switches. The related methods for each class are also defined. For example, the methods `doublegetG()`, `doublegetib()`, and `voidupdate(double&)` in CPElement class are used to obtain the element's equivalent conductance, calculate branch current, and update history current source, respectively. For storing electrical networks, several C++ structures are created in this program. The CBranch and CShunt structures include all branch-type and shunt-type elements in the network with all information such as the type, nodes names, and object of each element. Structures CIout, CVout and CSWNode are used to save current output, voltage output and switch information, respectively. All structures are stored in the predefined C++ vectors. Fig. 16(b) shows an example of  $RL$  branch in the C++ S-function hierarchy.

In order to make the C++ EMTP program applicable to generic electrical networks, ATP data files are used as standard input files for the S-function. In this fashion, the program is fully adaptable for different electrical networks. During this process, the ATP branch cards, switch cards, output cards, and source cards are read. As a result, all vectors and objects are initialized corresponding to the specific electrical network to be simulated.

The real-time EMTP simulation process begins with the pre-calculation of system admittance matrix  $\mathbf{Y}$  and its inverse  $\mathbf{Y}^{-1}$  corresponding to all the switching states. In each simulation

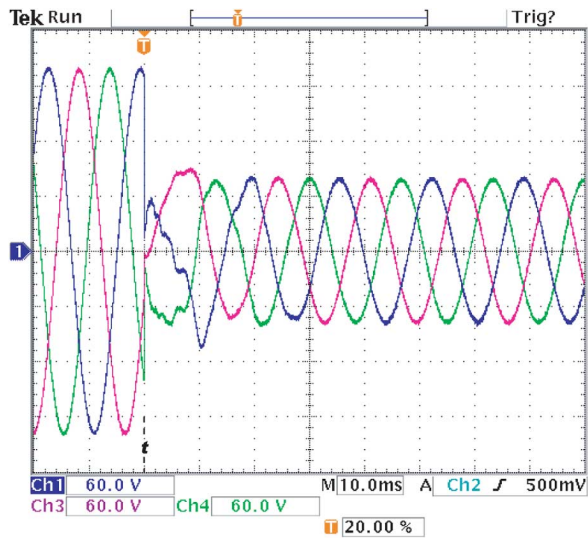


Fig. 17. Real-time oscilloscope traces showing three-phase voltages during a three-phase to ground fault transient at  $t = 0.05$  s at the Bus 524 of the AIES Area 50 ( $X$  axis scale: 1 div = 10 ms,  $Y$  axis scale: 1 div = 60 kV).

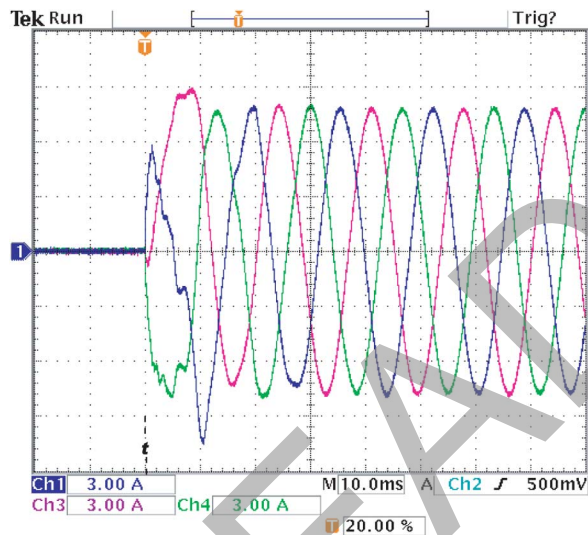


Fig. 18. Real-time oscilloscope traces showing three-phase fault currents during a three-phase to ground fault transient at  $t = 0.05$  s at the Bus 524 of the AIES Area 50 ( $X$  axis scale: 1 div = 10 ms,  $Y$  axis scale: 1 div = 3 kA).

time-step, switch states from the S-function block input are read and the matching  $Y^{-1}$  is retrieved from memory. Then the current source vector is obtained, nodal voltage vector is calculated and the history terms (current sources) are updated. Finally outputs requested in the ATP data file are sent to the S-function block output.

Figs. 17–20 show the transient waveforms captured by a real-time oscilloscope connected to the FPGA-based I/Os of the simulator. As can be observed, these results are indistinguishable from the off-line simulation results shown in Figs. 11–14.

## V. CONCLUSIONS

This paper proposed a new systematic approach for constructing a Robust Two-Layer Network Equivalent for external

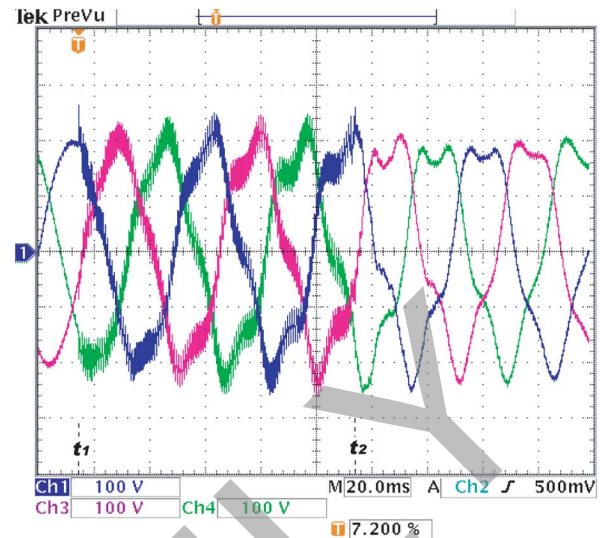


Fig. 19. Real-time oscilloscope traces showing three-phase voltages during a harmonic current injection transient between  $t_1 = 0.0331$  s and  $t_2 = 0.0664$  s at the Bus 524 of the AIES Area 50 ( $X$  axis scale: 1 div = 20 ms,  $Y$  axis scale: 1 div = 100 kV).

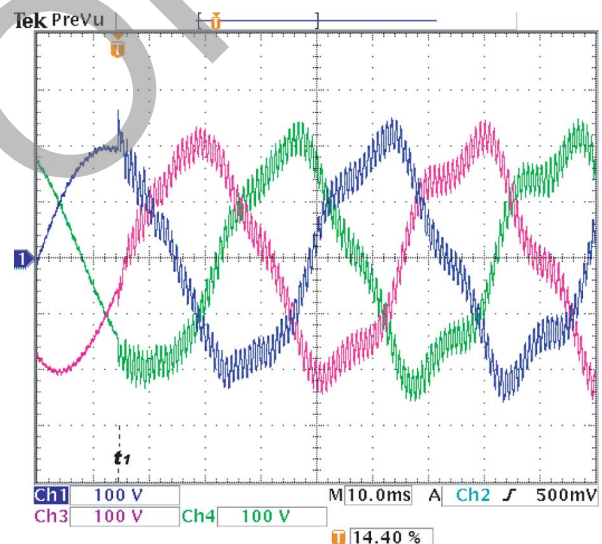


Fig. 20. Detailed view of transient in Fig. 19 ( $X$  axis scale: 1 div = 10 ms,  $Y$  axis scale: 1 div = 100 kV).

systems suitable for real-time electromagnetic transient simulation. The generated equivalent is of low-order and high accuracy compared to the full model in frequency-domain over a wide frequency range. The merits of this method are its robustness, its accuracy in not only transient frequencies but also at dc and power frequencies, and its optimal Deep Region order determination feature.

A case study of realistic large-scale power system-Alberta Interconnected Electric System-verified the effectiveness (accuracy and computational efficiency) of the Robust TLNE model vis-à-vis the full model, and the FDNE model. Off-line time-domain simulation in ATP validated the model performance. A real-time EMTP program was created to implement the transient simulation on a parallel PC-Cluster based real-time simulator. The real-time simulation results achieved are nearly identical

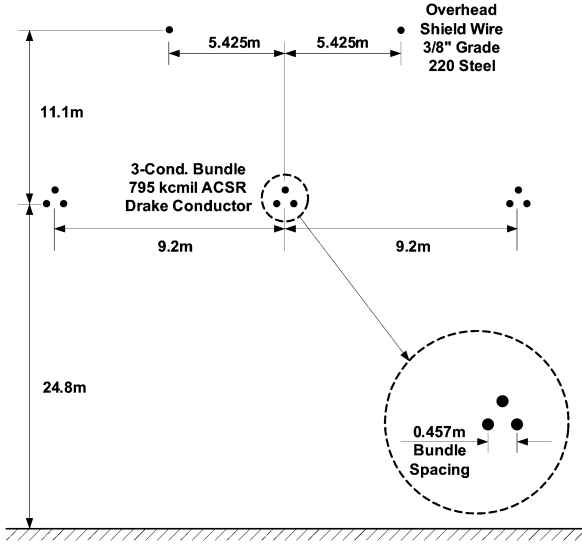


Fig. 21. Tower geometry for lines in the Surface Layer.

with the off-line simulation results from the full model. Future research directions in this area include how to automatically partition a system into the study zone and external system, and how to include unbalanced external systems especially those with untransposed transmission lines in the Surface Layer.

#### APPENDIX A CALCULATION OF JACOBIAN MATRIX $J(\omega)$

Consider a Surface Layer parameter  $\rho_s$  to be optimized, from (5), then the partial derivatives of input admittance with respect to  $\rho_s$  are given as follows:

$$\begin{aligned} \frac{\partial \tilde{Y}_{\text{input}}(s)}{\partial \rho_s} &= \frac{\partial \tilde{Y}_{AA}(s)}{\partial \rho_s} \\ &\quad - \frac{\partial \tilde{Y}_{AB}(s)}{\partial \rho_s} [\tilde{Y}_{BB}(s) + \tilde{Y}_{\text{deep}}(s)]^{-1} \tilde{Y}_{BA}(s) \\ &\quad - \tilde{Y}_{AB}(s) [\tilde{Y}_{BB}(s) + \tilde{Y}_{\text{deep}}(s)]^{-1} \frac{\partial \tilde{Y}_{BA}(s)}{\partial \rho_s} \\ &\quad + \tilde{Y}_{AB}(s) [\tilde{Y}_{BB}(s) + \tilde{Y}_{\text{deep}}(s)]^{-1} \frac{\partial \tilde{Y}_{BB}(s)}{\partial \rho_s} \\ &\quad * [\tilde{Y}_{BB}(s) + \tilde{Y}_{\text{deep}}(s)]^{-1} \tilde{Y}_{BA}(s). \end{aligned} \quad (12)$$

Partial derivatives of input admittance with respect to a Deep Region parameter  $\rho_d$  to be optimized can be obtained as

$$\begin{aligned} \frac{\partial \tilde{Y}_{\text{input}}(s)}{\partial \rho_d} &= \tilde{Y}_{AB}(s) [\tilde{Y}_{BB}(s) + \tilde{Y}_{\text{deep}}(s)]^{-1} \frac{\partial \tilde{Y}_{\text{deep}}(s)}{\partial \rho_d} \\ &\quad * [\tilde{Y}_{BB}(s) + \tilde{Y}_{\text{deep}}(s)]^{-1} \tilde{Y}_{BA}(s). \end{aligned} \quad (13)$$

Since the Deep Region parameters such as poles and residues are complex quantities, real and imaginary parts are treated separately in  $\partial \tilde{Y}_{\text{deep}}(s)/\partial \rho_d$ , as explained in [6].

TABLE II  
LENGTH OF TRANSMISSION LINES IN THE SURFACE LAYER

Line	1202L	1203L	1209L
Length (km)	68.85	18.26	67

#### APPENDIX B LINE GEOMETRY

Fig. 21 shows the typical tower geometry of lines in the Surface Layer. Table II shows the length of lines in the Surface Layer.

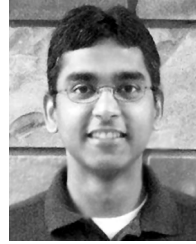
#### REFERENCES

- [1] H. W. Dommel, "Digital computer solution of electromagnetic transients in single and multiphase networks," *IEEE Trans. Power App. Syst.*, vol. PAS-88, pp. 388–399, Apr. 1969.
- [2] A. S. Morched and V. Brandwajn, "Transmission network equivalents for electromagnetic transients studies," *IEEE Trans. Power App. Syst.*, vol. PAS-102, pp. 2984–2994, Sep. 1983.
- [3] A. S. Morched, J. H. Ottevangers, and L. Marti, "Multi-port frequency dependent network equivalents for the EMTF," *IEEE Trans. Power Del.*, vol. 8, no. 3, pp. 1402–1412, Jul. 1993.
- [4] B. Gustavsen and A. Semlyen, "Rational approximation of frequency domain responses by vector fitting," *IEEE Trans. Power Del.*, vol. 14, no. 3, pp. 1052–1061, Jul. 1999.
- [5] B. Gustavsen and A. Semlyen, "Enforcing passivity for admittance matrices approximated by rational functions," *IEEE Trans. Power Syst.*, vol. 16, no. 1, pp. 97–104, Feb. 2001.
- [6] M. Abdel-Rahman, A. Semlyen, and M. R. Iravani, "Two-layer network equivalent for electromagnetic transients," *IEEE Trans. Power Del.*, vol. 18, no. 4, pp. 1328–1335, Oct. 2003.
- [7] X. Nie and V. Dinavahi, "A robust two-layer network equivalent for transient studies," in *Proc. Int. Conf. Power Syst. Transients (IPST)*, Montreal, QC, Canada, Jun. 2005, pp. 1–6.
- [8] X. Nie, "Real-time digital simulation of large power systems based on a robust two-layer network equivalent," M.Sc. thesis, Univ. Alberta, Edmonton, AB, Canada, 2005.
- [9] L. Pak, M. O. Faruque, X. Nie, and V. Dinavahi, "A versatile cluster-based real-time digital simulator for power engineering research," *IEEE Trans. Power Syst.*, vol. 21, no. 2, pp. 455–465, May 2006.
- [10] W. Scott-Meyer, *EMTP Theory Book*. Portland, OR: Bonneville Power Administration, 1984.
- [11] A. Chipperfield, P. Fleming, H. Pohlheim, and C. Fonseca, *Genetic Algorithm Toolbox Manual For MATLAB*. Sheffield, U.K.: Univ. Sheffield, 1994.
- [12] J. R. Marti, "Accurate modeling of frequency-dependent transmission lines in electromagnetic transient simulations," *IEEE Trans. Power App. Syst.*, vol. PAS-101, pp. 147–155, Jan. 1982.
- [13] L. Marti, "Low-order approximation of transmission line parameters for frequency-dependent models," *IEEE Trans. Power App. Syst.*, vol. PAS-102, pp. 3582–3589, Nov. 1983.
- [14] A. B. Fernandes and W. L. A. Neves, "Transmission lines: Fitting technique optimization," in *Proc. Int. Conf. Power Syst. Transients (IPST)*, Seattle, WA, Jun. 22–26, 1997.
- [15] X. Wang and R. M. Mathur, "Real-time digital simulator of the electromagnetic transients of transmission lines with frequency dependence," *IEEE Trans. Power Del.*, vol. 4, no. 4, pp. 2249–2255, Oct. 1989.
- [16] C. Dufour, H. Le-Huy, J. Soumagne, and A. E. Hakimi, "Real-time simulation of power transmission lines using marti model with optimal fitting on dual-dsp card," *IEEE Trans. Power Del.*, vol. 11, no. 1, pp. 412–419, Jan. 1996.
- [17] RT-LAB 8.0 user manual Opal-RT Technologies, Inc., Montreal, QC, Canada, 2006.
- [18] MATLAB user's guide, The MathWorks, Inc., Natick, MA, 1998.



**Xin Nie** (S'04) received the B.Eng. degree in electrical engineering from the Northeastern University, China, in 1997, and the M.Sc. degree in electrical engineering from the University of Alberta, Edmonton, AB, Canada, in 2005.

He worked as a Transmission Line Design Engineer in China from 1997 to 2001. Currently, he is a Line Technical Professional with SNC-Lavalin T & D, Calgary, AB, Canada. His research interests include electromagnetic transient simulation and real-time simulation of power systems as well as insulation air gaps and coordinations.



**Venkata Dinavahi** (M'00) received the Ph.D. degree from the University of Toronto, Toronto, ON, Canada, in 2000.

Presently, he is an Associate Professor with the University of Alberta, Edmonton, AB, Canada. His main research interests are in the areas of real-time simulation, electromagnetic transients, power electronics, and digital control.



**Yuan Chen** (S'06) received the B.Sc. and M.Sc. degrees in electrical engineering from Hunan University, China, in 1992 and 2000, respectively. Currently, he is pursuing the M.Sc. degree at the Department of Electrical and Computer Engineering, University of Alberta, Edmonton, AB, Canada.

He worked as a Electrical Engineer in China. His research interests include application of microprocessors and real-time simulation of power systems.

READ ONLY